



Optics Letters

Magneto-optic trap using a reversible, solid-state alkali-metal source

S. KANG,^{1,2,3,*} K. R. MOORE,¹ J. P. MCGILLIGAN,^{1,2} R. MOTT,⁴ A. MIS,⁴ C. ROPER,⁴
E. A. DONLEY,¹ AND J. KITCHING¹

¹National Institute of Standards and Technology, Boulder, Colorado 80305, USA

²University of Colorado, Department of Physics, Boulder, Colorado 80309, USA

³Key Laboratory of Atomic Frequency Standards, Wuhan Institute of Physics and Mathematics, Chinese Academy of Sciences, Wuhan 430071, China

⁴HRL Laboratories, LLC; Malibu, California 90265, USA

*Corresponding author: kangsongbai@wipm.ac.cn

Received 25 March 2019; revised 30 April 2019; accepted 5 May 2019; posted 8 May 2019 (Doc. ID 363303); published 6 June 2019

We demonstrate a novel way to form and deplete a vapor-cell magneto-optic trap (MOT) using a reversible, solid-state alkali-metal source via an applied polarized voltage. Using ~100 mW of electrical power, a trapped-atom number of 5×10^6 has been achieved, starting from near zero and the timescales of the MOT formation and depletion of ~1 s. This fast, reversible, and low-power alkali-atom source is desirable in both tabletop and portable cold-atom systems. The core technology of this device should translate readily to other alkali and alkaline-earth elements that could find a wide range of uses in cold-atom systems and instruments. © 2019 Optical Society of America

<https://doi.org/10.1364/OL.44.003002>

Laser cooling has revolutionized atom-based sensors and instrumentation. The low temperature of the atoms allows for long interaction periods and narrow spectroscopic linewidths that are critical for precision measurements. In all cold-atom systems, a source of (warm) atoms is required to provide an appropriate atom density for forming the magneto-optic trap (MOT). Commercial rubidium (Rb) and cesium (Cs) alkali-metal dispensers (AMDs) have been widely used in laboratory-based cold-atom experiments for decades due to their reliability and long lifetimes [1]. However, these AMDs release alkali atoms via resistive heating, often requiring several watts during operation. Furthermore, dispensing via resistive heating is a non-reversible process; once the alkali metal is created, it cannot be recovered by the dispenser. Non-reversible alkali sources can be problematic, for example, when trying to maintain a constant alkali vapor density in a cold-atom apparatus over a wide range of ambient temperatures. At low temperatures, the alkali vapor pressure in the system drops, and a higher flux of atoms from the source is required. If the apparatus temperature subsequently increases, those atoms must be removed from the system by pumping, resulting in rapid depletion of the source material upon repeated temperature cycling. This type

of dispensing not only hinders the ability to precisely control the alkali-atom density for a cold-atom system over a large environmental temperature range, but also results in a long time constant for the alkali-atom density to decay, which negatively impacts the cycling rate, and hence performance, of cold-atom metrological experiments [2–4]. Such effects limit the use of AMDs in field-deployable, long-lifetime compact cold-atom sensors and clocks [5,6].

On the other hand, techniques like laser-ablated or current-pulsed AMDs, light-induced atomic desorption (LIAD), and cold fingers have been developed to considerably enhance the possibilities of modulating alkali-atom density in cold-atom systems [7–14]. However, none of these techniques simultaneously meet the requirements of being fast, reversible, low-power, and able to be miniaturized, which are important for developing a portable cold-atom physics package.

Recent efforts have focused on novel solid-state alkali sources that operate via an electrolysis process [15,16]. A promising candidate material for this process is a beta double-prime alumina (β'' -alumina) ceramic, which features a high ionic mobility for alkali ions. By utilizing an applied voltage to control the flux of mobile alkali ions within the ceramic, this device has previously demonstrated bidirectional vapor-phase Rb sourcing and sinking functionality [17–19]. In this Letter, we describe the novel implementation of a voltage-controlled, solid-state β'' -alumina Rb alkali-metal source (AMS) to demonstrate the formation and depletion of a Rb MOT in a vapor cell.

As shown in Fig. 1, our experimental measurements are carried out in a standard six-beam MOT configuration [20,21]. The cooling and repumping light are derived from a single frequency-stabilized distributed-Bragg-reflector laser phase-modulated at 2.9 GHz. The carrier light is optically red-detuned by approximately two linewidths from the $^{85}\text{Rb } 5S_{1/2}(F=3) \rightarrow 5P_{3/2}(F'=4)$ cooling transition, fiber-coupled to the experiment, and collimated with a $1/e^2$ diameter of 3.8 mm and optical power of 4 mW in each of the six beams. Our ultra-high-vacuum system includes a standard 10 mm by 10 mm cross-sectional-area vapor cell and a 2 L/s ion pump.

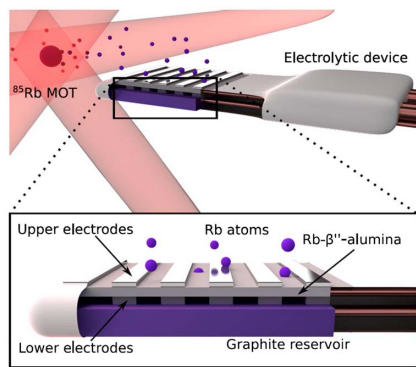


Fig. 1. Sketch of the experimental set-up with the six-beam MOT and in-vacuum electrolytic device. Inset: illustrated cross-section of solid-state Rb AMS.

The cell walls are coated with octadecyltrichlorosilane (OTS) to minimize alkali adsorption on the wall surface. Furthermore, a Rb AMS is installed in the vacuum system to initially load the AMS reservoir. Before the introduction of alkali metal into the chamber, the background pressure is $\sim 1 \times 10^{-7}$ Torr, which could be reduced by more thorough vacuum procedures, such as baking at an elevated temperature.

A CCD camera (timing resolution of 100 ms per data point) collects fluorescence images of the MOT with a spatial resolution of $17 \mu\text{m}$. The trapped-atom number and the vapor-phase Rb density are estimated based on the MOT and background fluorescence intensity levels on the camera images, respectively.

The AMS is mounted inside the vapor cell about 1 cm from the intersection of the MOT beams. In the inset of Fig. 1, we show an illustrated cross-section of the AMS. The active surface area is $7.5 \text{ mm} \times 14.5 \text{ mm}$, and the thickness is approximately 2 mm. The solid-state electrolyte is sandwiched between grids of surface electrodes composed of fine Ti/Pt fingers with the top electrode having a period of $1 \mu\text{m}$ and with the lower electrodes in contact with a graphite reservoir. The high spatial density of the electrode fingers not only increases the atom-electrode contact area to aid electrochemical oxidation of Rb atoms, but also supports the efficient transport of ionizable atoms into the electrolyte. The lower electrodes and the graphite reservoir are sealed by a vacuum-compatible epoxy to isolate the stored Rb atoms from the cell environment. Heater wires buried inside the epoxy heat the AMS to approximately 100°C with a power consumption of $\sim 100 \text{ mW}$, which both increases the desorption rate of Rb atoms from the device surface and helps improve ionic mobility within the electrolyte to enlarge the Rb sinking/sourcing dynamic range. A voltage is applied through a $4.6 \text{ k}\Omega$ series resistor and the electrodes of the AMS. Depending on this voltage polarity, the AMS can reversibly source or sink Rb atoms from the vapor in the cell. No obvious Rb emission was detected when the AMS was operated at room temperature.

Prior to initial operation, the Rb AMS is operated for several hours to fill the vapor cell with Rb vapor. Then, a negative voltage is applied to the AMS for half an hour to load the graphite reservoir with Rb. After this Rb pre-loading process, we turn off the AMS and wait for the Rb density in the vapor cell to decay to a level such that the MOT signal drops below the detection threshold of the camera.

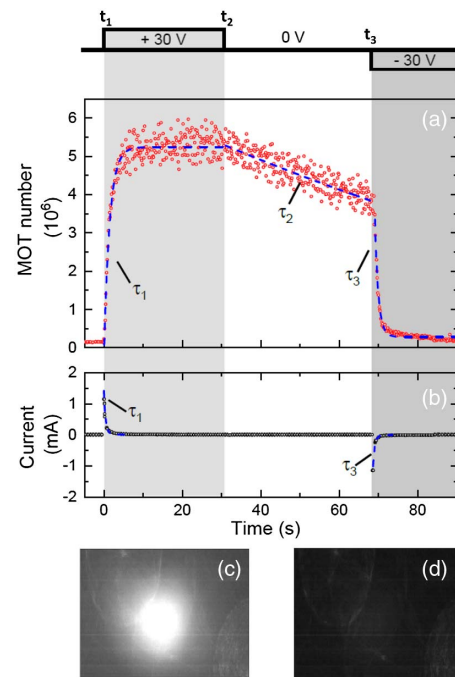


Fig. 2. Demonstration of MOT formation and depletion using the device. (a) The dynamic behavior of the trapped-atom number (red points) as the voltage on the device is changed. The number of trapped atoms is extracted from raw CCD image data by fitting to a two-dimensional Gaussian function. (b) The corresponding current flowing through the device (black points). The labelled gray and white regions indicate periods of different voltages applied to the AMS: (1) $+30 \text{ V}$ for $t_1 < t < t_2$; (2) 0 V for $t_2 < t < t_3$; and (3) -30 V for $t > t_3$. (c) CCD image of the MOT at $\sim 20 \text{ s}$. (d) CCD image of the MOT at $\sim 90 \text{ s}$.

In Fig. 2(a), we demonstrate MOT formation and depletion controlled solely via the voltage applied across the Rb AMS. The demonstration is divided into three periods. First, the voltage is set to $+30 \text{ V}$ ($t_1 \leq t < t_2$). When the voltage is applied ($t = t_1$), the trapped-atom number increases from a near-zero baseline to a maximum level of $N_{\text{MOT}} \sim 5 \times 10^6$ with a single time constant τ_1 of $\sim 1 \text{ s}$. An image of the MOT at this maximum fluorescence level is shown in Fig. 2c. Next, the voltage is decreased to 0 V ($t_2 \leq t < t_3$). A slow decay of the number of trapped atoms is observed with a time constant $\tau_2 \sim 100 \text{ s}$. Finally, the voltage is reversed to -30 V ($t \geq t_3$). The number of trapped atoms falls rapidly with a depletion time constant τ_3 of $\sim 1 \text{ s}$. An image of the MOT at the end of the cycle with the voltage reversed is shown in Fig. 2d. The cooling beams and trap magnetic fields are on throughout. Because the non-Rb background pressure was $\sim 1 \times 10^{-7}$ Torr, the time constants for the MOT loading process were less than 100 ms for all Rb vapor densities and, hence, did not limit the dynamic behavior of the trapped atoms in our experiment.

We were able to monitor the background Rb density to some extent by measuring the change in the light captured on the CCD around the edges of the image where the cold-atom fluorescence was low. We observed changes in the Rb density that roughly corresponded to the MOT number shown in Fig. 2(a), but with time constants τ_1 and τ_3 are about 30% longer than the MOT time constants. This may suggest some

weak saturation of the cold-atom number at the higher background alkali densities.

The current, as shown in Fig. 2(b), measures the transport of Rb ions across the electrolyte. Those Rb ions ultimately either plate out as Rb metal on the device surface or accumulate behind the electrodes. During the first period ($t_1 < t < t_2$), the current exhibits a rapid decay with a time constant of 0.4(1) s, likely due to electrode polarization, and then evolves into a slow decay. The positive initial spike (~ 1 mA at $t \sim t_1$) indicates a high Rb ion transport rate ($\sim 10^{16}$ ions/s) from the graphite reservoir through the ionic conductor. If all of those Rb ions were to recombine with electrons and desorb as vapor-phase Rb atoms, a much higher Rb density ($\sim 10^{15}/\text{cm}^3$) would be yielded in the cell volume (~ 10 cm³) than is observed. Thus, it is likely that most of the Rb ions conducted through the electrolyte either accumulate behind the electrodes or form a Rb metal thin film on the AMS surface rather than immediately desorbing into the vapor. The subsequent low current (~ 10 μ A for 2 s $< t < t_2$) likely indicates a slow rate of Rb atom plating on the surface. This step would result in a Rb saturated vapor pressure ($\sim 10^9$ atoms/cm³) for the MOT loading in the vapor cell. The current during the third period ($t_3 < t$) exhibits a negative initial spike (~ -1 mA at $t \sim t_3$) with a decay time constant of 0.4(1) s followed by a low negative current (~ -10 μ A at 70 s $< t$). The negative current spike indicates a high Rb ion transport rate, presumably removing any Rb accumulated beneath the electrodes and most of the Rb metal film still on the surface. The low current is likely due to subsequent sinking from any remaining Rb metal film and from the vapor-phase Rb. The current dynamic (τ_1 and τ_3) is faster than the trapped-atom number and Rb vapor density because of the additional Rb atom desorption/adsorption process. The current time constants might be limited by the effective electrical contact resistance between the accumulated ions and the electrodes. This capability to rapidly sink Rb is a unique feature that distinguishes this electrochemical AMS from traditional AMDs. We note that the peak power for Rb sinking and sourcing is only ~ 10 mW, much lower than the heating power.

This work presents a new mechanism for manipulating the vapor-cell cold-atom samples by utilizing a solid-state electrochemical Rb AMS. In Table 1, we compare the characteristics of the vapor-cell MOT formed using different Rb sources. Using the AMS, a trapped-atom number of $\sim 5 \times 10^6$ has been achieved from a near-zero MOT background. The maximum MOT number achievable could be further improved if the background gas pressure was lower. Such a high dynamic range

Table 1. Characteristics of a Vapor-Cell MOT Formed by Different Rb Sources

	MOT				Reversible Operation
	Dynamic Range	Depletion Time (s)	Operation Method	Power	
AMS	High	~ 1	Voltage	~ 100 mW	Yes
AMD ^a	High	~ 10	Current	~ 1 W	No
LIAD ^b	Low	~ 10	LED	~ 10 W ^c	No

^aSee Ref. [8].

^bSee Ref. [12].

^cSee Ref. [22].

can be obtained by the pulsed AMD technique but not by LIAD. Generally, there is a tradeoff between a high dynamic range and a fast depletion time for alkali-atom vapor pressure [22]. However, due to the unique active-reversible function of the AMS, the MOT depletion time constant can be as fast as ~ 1 s in our apparatus. Dugrain *et al.* have obtained a 100 ms vapor-pressure modulation period in a pulsed AMD set-up, but that system requires an external, additional apparatus to thermally sink the alkali vapor [9]. Due to the electrochemical operating principle of the AMS, both sourcing and sinking functions are achieved by simply applying a voltage across the compact, in-vacuum package. Moreover, the AMS operates with a power of only ~ 100 mW limited by heating, which is critical for use in a portable, battery-powered instrument. The capacity of AMS could be as high as ~ 1 μ g after a half-hour pre-loaded process, which can guarantee a long lifetime for a cold-atom microsystem. Likewise, the planar design of the AMS is conducive to system integration and mass fabrication.

In summary, this compact device meets some requirements for field-deployable cold-atom systems, potentially allowing MOT operation over a range of ambient temperatures. Meanwhile, the AMS could also find applications in experiments like those requiring evaporative cooling, where large numbers of atoms could be loaded into magnetic traps at high atomic density, and, subsequently, long trap lifetimes could be obtained by lowering the density [23]. The micro-fabrication of this device complements mass production and implementation with other compact cold-atom devices to enable increased MOT number control and stability in future quantum technologies [5,24,25]. The AMS pre-loaded with Rb is potentially able to replace the commercial AMDs in the future, further simplifying vacuum assemblies and allowing for lower-power operation. Additionally, the core technology of the device should translate readily to other alkali and alkaline-earth elements that find a wide range of uses in cold-atom systems.

Funding. Defense Advanced Research Projects Agency (DARPA); Space and Naval Warfare Systems Center Pacific (SSC Pacific) (N66001-15-C-4027).

Acknowledgment. The authors acknowledge DARPA program manager Robert Lutwak as well as Logan Sorenson, Matthew Rakher, Jason Graetz, John Vajo, Adam Gross, and Danny Kim of HRL Laboratories, LLC for useful discussions. We further acknowledge Florian Herrault, Geovanni Candia, Stephen Lam, Tracy Boden, Margie Cline, Ryan Freeman, and Lian-Xin Coco Huang for assistance with device fabrication. This work is a contribution of NIST, an agency of the U.S. government, and is not subject to copyright. J. P. M gratefully acknowledges support from the English Speaking Union and Lindemann Fellowship.

REFERENCES

1. M. Succi, R. Canino, and B. Ferrario, *Vacuum* **35**, 579 (1985).
2. C. Wieman, G. Flowers, and S. Gilbert, *Am. J. Phys.* **63**, 317 (1995).
3. U. D. Rapol, A. Wasan, and V. Natarajan, *Phys. Rev. A* **64**, 023402 (2001).
4. S. Bartalini, I. Herrera, L. Consolino, L. Pappalardo, N. Marino, G. D'Arrigo, and F. Cataliotti, *Eur. Phys. J. D* **36**, 101 (2005).
5. J. A. Rushton, M. Aldous, and M. D. Himsworth, *Rev. Sci. Instrum.* **85**, 121501 (2014).

6. J. Kitching, E. A. Donley, S. Knappe, M. Hummon, A. T. Dellis, J. Sherman, K. Srinivasan, V. A. Aksyuk, Q. Li, D. Westly, B. Roxworthy, and A. Lal, *J. Phys. Conf. Ser.* **723**, 012056 (2016).
7. P. F. Griffin, K. J. Weatherill, and C. S. Adams, *Rev. Sci. Instrum.* **76**, 093102 (2005).
8. J. Fortagh, A. Grossmann, T. W. Hänsch, and C. Zimmermann, *J. Appl. Phys.* **84**, 6499 (1998).
9. V. Dugrain, P. Rosenbusch, and J. Reichel, *Rev. Sci. Instrum.* **85**, 083112 (2014).
10. A. Bogi, C. Minelli, A. Burchianti, E. Mariotti, L. Moi, S. Gozzini, L. Marmugi, and A. Lucchesini, *Opt. Lett.* **34**, 2643 (2009).
11. T. Karaulanov, M. T. Graf, D. English, S. M. Rochester, Y. J. Rosen, K. Tsigutkin, D. Budker, E. B. Alexandrov, M. V. Balabas, D. F. J. Kimball, F. A. Narducci, S. Pustelny, and V. V. Yashchuk, *Phys. Rev. A* **79**, 012902 (2009).
12. L. Torralbo-Campo, G. D. Bruce, G. Smirne, and D. Cassettari, *Sci. Rep.* **5**, 14729 (2015).
13. G. Telles, T. Ishikawa, M. Gibbs, and C. Raman, *Phys. Rev. A* **81**, 032710 (2010).
14. K. Moore, T. Purdy, K. Murch, S. Leslie, S. Gupta, and D. Stamper-Kurn, *Rev. Sci. Instrum.* **76**, 023106 (2005).
15. F. Gong, Y.-Y. Jau, K. Jensen, and W. Happer, *Rev. Sci. Instrum.* **77**, 076101 (2006).
16. J. J. Bernstein, S. Feller, A. Ramm, J. North, J. Maldonis, M. Mescher, W. Robbins, R. Stoner, and B. Timmons, *Solid State Ion.* **198**, 47 (2011).
17. J. J. Bernstein, A. Whale, J. Brown, C. Johnson, E. Cook, L. Calvez, X. Zhang, and S. W. Martin, *Proceedings of the Solid-State Sensors, Actuators and Microsystems Workshop*, Hilton Head Island, South Carolina (2016), pp. 180–184.
18. S. Kang, R. P. Mott, K. A. Gilmore, L. D. Sorenson, M. T. Rakher, E. A. Donley, J. Kitching, and C. S. Roper, *Appl. Phys. Lett.* **110**, 244101 (2017).
19. S. Kang, R. P. Mott, A. V. Mis, C. S. Roper, E. A. Donley, and J. Kitching, *Opt. Express* **26**, 3696 (2018).
20. E. L. Rabb, M. Prentiss, A. Cable, S. Chu, and D. E. Pritchard, *Phys. Rev. Lett.* **59**, 2631 (1987).
21. C. Monroe, W. Swann, H. Robinson, and C. Wieman, *Phys. Rev. Lett.* **65**, 1571 (1990).
22. G. Bruce, University of St Andrews, North Haugh, St Andrews, Scotland, UK (personal communication, 2018).
23. B. P. Anderson and M. A. Kasevich, *Phys. Rev. A* **63**, 023404 (2001).
24. D. T. Argyrios, M. T. Hummon, S. Kang, E. A. Donley, and J. Kitching, *Frontiers in Optics* (2016).
25. J. P. McGilligan, P. F. Griffin, R. Elvin, S. J. Ingleby, E. Riis, and A. S. Arnold, *Sci. Rep.* **7**, 384 (2017).